cosmetics

MDPI

Article

Yeast–Plant-Derived Consortia Factors Exhibit an Enriched Extracellular Metabolome with Antioxidant and Anti-Inflammatory Potential in Human Skin-Derived Cells

Assaf Zemach *, Mikhail R. Plaza, Melissa Palomares, Dior Simmons, Bong Seop Lee, Dodanim Talavera-Adame and Nathan Newman *

Rinati Labs, Hawthorne, CA 90250, USA
* Correspondence: dr.zemach@rinatilabs.com (A.Z.); doctor@nathannewmanmd.com (N.N.)

Abstract

Cells secrete metabolites and other bioactive factors into the extracellular environment, collectively known as the secretome. While single-species secretomes are well studied, the impact of interspecies co-culture on secretome composition remains poorly understood. Here, we investigated whether co-culturing plant and yeast cells could generate emergent secretory outputs. A yeast suspension of *Ustilago cynodontis* was co-cultured with plant cells derived from *Ocimum sanctum* (Tulsi) to produce a novel set of secretory factors termed Consortia Factors (CFx). Metabolomic profiling of the Ustilago-Tulsi CFx, termed CFx-α1, revealed a metabolome that was distinct from and more enriched than those of either monoculture. Statistical clustering demonstrated divergence from single-culture secretomes, with approximately one-third of enriched metabolites absent from either organism grown alone. Using an algorithm designed to identify validated antioxidant and anti-inflammatory metabolites, we found that CFx-α1 was significantly enriched in these metabolites, including vitamin C. Consistent with this profile, CFx-α1 exhibited greater intracellular antioxidant activity and more effectively attenuated lipopolysaccharide (LPS)-induced NF-κB nuclear localization in human skin-derived cells than either single-culture conditioned medium. CFx-α1 also maintained human dermal fibroblast viability across concentrations of 1–5%. These findings indicate that plant–yeast co-culture generates a distinct and functionally enriched extracellular metabolome with antioxidant and anti-inflammatory potential, highlighting consortia-based culture systems as a promising strategy for producing bioactive metabolites for cosmetic applications.

Keywords: secretome; co-culture; plant–yeast interactions; bioactive metabolites; antioxidant activity

Check for updates

Academic Editor: Othmane Merah

Received: 18 August 2026
Revised: 21 October 2026
Accepted: 21 October 2026
Published: 26 October 2026

Copyright: © 2026 by the authors. Licensee MDPI, Basel, Switzerland. This article is an open access article distributed under the terms and conditions of the Creative Commons Attribution (CC BY) license.

1. Introduction

The secretome is the complete set of biochemical factors secreted by cells into the extracellular space [1]. It plays essential roles in numerous biological processes and interactions [2]. A significant component of the secretome is metabolites—low-molecular-weight molecules that function as key intermediates and products of metabolism. These include sugars, amino acids, lipids, nucleotides, organic acids, vitamins, hormones, flavonoids, phenolics, and glucosinolates. Advances in analytical technologies have greatly improved the detection and quantification of these metabolites, enabling detailed investigation of metabolic networks and cellular physiology [3].

Plants and fungi synthesize a wide range of metabolites that contribute significantly to human health. Yeast, for example, produces both primary and secondary metabolites with major industrial relevance. These include biofuels such as bioethanol, organic acids, hydrolytic enzymes, vitamins, amino acids, and antibiotics, which are products vital to the food, agricultural, and pharmaceutical sectors [4]. Plant cell suspension cultures have also emerged as a valuable biotechnological platform for producing high-value secondary metabolites used in pharmaceuticals, cosmetics, and food. Such cultures offer key advantages: controlled production conditions, independence from climate and soil, and year-round yields of consistent quality and quantity [5–7]. The secretome of plant cell suspensions, which include extracellular proteins and metabolites, is central to these processes. Because it can be separated from cells without disruption, the secretome provides a continuous and reliable source of extracellular proteins essential for cell wall remodeling and stress defense [8].

Plant-derived extracts, plant cell-culture products, and microbial ferments are increasingly used in cosmetic formulations as sources of bioactive compounds with antioxidant, moisturizing, soothing, skin-conditioning, and anti-aging properties [9,10]. During microbial fermentation of plant-derived material, microorganisms biotransform plant constituents through enzymatic reactions, converting larger or conjugated molecules into smaller and potentially more bioavailable metabolites [11]. These transformations can alter the chemical composition, polarity, solubility, stability, and biological activity of the resulting material, while also generating new microbial- or plant-derived metabolites [10,11]. Consequently, fermented plant-derived ingredients may exhibit physicochemical and biological properties distinct from the original plant material and are increasingly explored as active ingredients for antioxidant, anti-inflammatory, moisturizing, brightening, and other dermocosmetic applications [9–11]. This growing use of biotechnology-derived ingredients is also reflected by the inclusion of numerous plant- and fermentation-derived materials in the European Union CosIng database [10].

The potential of interspecies cell cultures has been increasingly recognized. For instance, endophytic fungi inhabit plant tissues in symbiosis and produce diverse bioactive compounds with health benefits such as antioxidant, anti-inflammatory, antimicrobial, and anticancer activities [12]. Similarly, microalgae–yeast co-cultivation creates a symbiotic system that produces valuable biofuels by sharing nutrients and metabolic byproducts, thereby enhancing overall lipid and biomass productivity for sustainable energy [13]. These examples affirm the benefits of interspecies co-culturing for metabolite production.

The Tulsi plant (*Ocimum tenuiflorum*/*sanctum*), also known as Holy basil, is a revered herb in traditional medicine, particularly in Ayurveda. Its leaves contain diverse compounds—including phenolics, flavonoids, and terpenoids—that contribute to pharmacological activities such as anti-stress, anticancer, antioxidant, and antidiabetic effects [14,15]. The fungus *Ustilago cynodontis* (hereafter referred to as Ustilago), a member of the Ustilaginaceae family, is typically known as a plant pathogen but also holds biotechnological importance [16,17]. It produces bioactive compounds such as the organic acid itaconate and mannosylerythritol lipids, which have applications in cosmetics, polymers, and biosurfactants [18,19]. Given the metabolic diversity observed in related Ustilaginaceae species [20], *U. cynodontis* remains a promising source for the discovery of additional bioactive compounds. In this study, untargeted metabolomics was applied to analyze and quantify the global effects of the secretome derived from an integrated cell suspension of the fungus *U. cynodontis* and the plant *O. sanctum*. The findings from the Ustilago–Tulsi co-culture, compared with either single culture or with a simple combination of their respective secretomes, demonstrate that CFx-α1 yields a unique and significantly enriched repertoire of beneficial bioactive compounds.

2. Materials and Methods

2.1. Biological Materials

Tulsi stem cell culture (callus) was established from an *O. sanctum* plant using plant growth hormones. The fungus *U. cynodontis* used in this study was isolated from a local bermudagrass (*Cynodon dactylon*) plant and was identified by its Internal Transcribed Spacer (ITS) sequence. *U. cynodontis* was cultivated in its yeast life cycle phase. ITS and whole-genome sequencing verified the identity of the fungus as *U. cynodontis*.

2.2. Growth Conditions

Ustilago and Tulsi cell cultures were cultivated in flasks containing Murashige and Skoog (MS) basal medium with vitamins (M519, PhytoTechnology Laboratories, Lenexa, KS, USA) at 4.43 g/L. The macronutrients in the medium were ammonium nitrate (1650 mg/L), potassium nitrate (1900 mg/L), calcium chloride, anhydrous (332.2 mg/L), magnesium sulfate, anhydrous (180.7 mg/L), and monobasic potassium phosphate (170 mg/L). Micronutrients included boric acid (6.2 mg/L), manganese sulfate monohydrate (16.9 mg/L), zinc sulfate heptahydrate (8.6 mg/L), potassium iodide (0.83 mg/L), sodium molybdate dihydrate (0.25 mg/L), cupric sulfate pentahydrate (0.025 mg/L), cobalt chloride hexahydrate (0.025 mg/L), ferrous sulfate heptahydrate (27.8 mg/L), and disodium EDTA dihydrate (37.26 mg/L). The medium also contained myo-inositol (100 mg/L), glycine (2 mg/L), nicotinic acid (0.5 mg/L), pyridoxine-HCl (0.5 mg/L), and thiamine-HCl (0.1 mg/L). The medium was supplemented with 3% sucrose and plant growth hormones (0.5 mg/L 2,4-dichlorophenoxyacetic acid and 0.5 mg/L kinetin). All cultures contained 50 mL of medium. Tulsi cultures were inoculated with 5 g of callus, Ustilago cultures with 4×10^7 cells, and Ustilago–Tulsi co-cultures with 5 g of Tulsi cells and 4×10^7 Ustilago cells [21]. Flasks were shaken at 120 rpm on an orbital shaker at room temperature (25 °C ± 1 °C). Based on our prior cultivation experience with *U. cynodontis*, a 7-day cultivation period was selected because it corresponds approximately to the late-log/early-stationary phase under these conditions. Growth at harvest was measured by biomass fresh weight and sugar consumption. Following seven days of cultivation, culture media were separated from the cells by centrifugation at 4700× *g* for 10 min at room temperature and stored at −80 °C. Conditioned media used for the human-cell assays were additionally filtered through a 0.22-µm filter. Three biological replicates were generated for each of the cultures: Tulsi, Ustilago, and Ustilago–Tulsi.

2.3. Ustilago Genome Sequencing

DNA extraction was performed on *U. cynodontis* cell pellets using the Genologue Universal Microbiome Extraction Kit (Genologue, Tucker, GA, USA), following the manufacturer's instructions. Library construction was carried out according to standard Illumina TruSeq chemistry using a modified KAPA HyperPrep kit and protocol. DNA was mechanically sheared to approximately 400 bp (peak size) by ultrasonication using a Bioruptor sonicator (Diagenode, Denville, NJ, USA). Approximately 100 ng of fragmented DNA first underwent an end-repair reaction to form blunt ends, followed by an A-tailing reaction to add 3′-A overhangs. A shortened version of Y-shaped adapters was then ligated to the DNA ends. Following bead-based double-sided size selection (Genologue, Tucker, GA, USA), the DNA libraries were amplified using primers to incorporate Unique Dual Indexes (UDI, Eurofins Genomics, Louisville, KY, USA) at both ends. The resulting libraries were normalized, pooled, and sequenced on a NovaSeq 6000 sequencer (Illumina, San Diego, CA, USA) for paired-end 150 bp reads.

The resulting genomic data were subjected to quality control to remove low-quality reads and adapter sequences and then aligned to a reference *U. cynodontis* genome [22]

using the BWA short-read aligner [23]. Variant calling was performed using *bcftools* [24] to identify SNPs, insertions, and deletions. The program CNVkit [25] was used to determine any copy number variation between our strain and the reference genome. The BRAKER2 pipeline was used to annotate and predict genes using gene prediction tools GeneMark-ES and AUGUSTUS [26,27]. To determine the effect of mutation, indels, and copy number variants (CNVs) on predicted genes, the program SnpEff [28] was used to predict their functional effect. Finally, a phylogenetic tree using SANS serif [29] was created to confirm our strain's relatedness to the *U. cynodontis* reference genome.

2.4. Metabolomic Analysis

Conditioned media derived from the three biological cultures of Ustilago, Tulsi, and Ustilago–Tulsi, collected and stored as described in Section 2.2, were submitted for untargeted metabolomics at the Carver Metabolomics Core, University of Illinois Urbana–Champaign Roy J. Carver Biotechnology Center (Urbana, IL, USA). After thawing, 95 µL of each conditioned-media sample was supplemented with 5 µL of internal standard mixture, vortexed, and 5 µL was injected onto the instrument for analysis. LC–MS analysis and data processing followed the workflow described previously in Zemach et al. [30], with the parameters detailed below. Samples were analyzed using a Dionex Ultimate 3000 series UHPLC system (Thermo Scientific, Waltham, MA, USA) coupled to a Q-Exactive MS system (Thermo Scientific), as described previously [31]. Samples were analyzed by reversed-phase liquid chromatography (RPLC) using a Waters Acquity ethylene-bridged hybrid (BEH) C18 column (100 mm × 2.1 mm, 1.7 µm) maintained at 25 °C with a flow rate of 0.3–0.4 mL/min (Waters Corp, Milford, MA, USA). The mobile phases consisted of (A) water with 0.1% formic acid and (B) acetonitrile with 0.1% formic acid. Spectra were acquired in both positive and negative ionization modes.

All LC–MS raw data files were processed using MS-DIAL v4.90 for data collection, peak detection, alignment, adduct assignment, and compound identification [32]. The detailed parameter settings were as follows: MS1 tolerance, 0.005 Da; MS2 tolerance, 0.01 Da; minimum peak height, 10,000 amplitude units; mass slice width, 0.05 Da; smoothing method, linear weighted moving average; smoothing level, 3 scans; minimum peak width, 5 scans. $[M - H]^-$, $[2M - H]^-$ and $[M + H]^+$, $[2M + H]^+$, $[M + NH4]^+$, $[M + Na]^+$, $[M + 2H]^{2+}$ were included as adducts in negative and positive modes, respectively. Compounds were annotated by m/z, MS/MS spectra, and retention time against an in-house library generated from chemical standards. In addition, they were annotated by m/z and MS/MS spectra using the public libraries MassBank of North America (MoNA), MassBank Europe (MassBank EU), and Global Natural Products Social Molecular Networking (GNPS), as well as the commercial library National Institute of Technology 20 (NIST20). Internal standards were monitored for retention time and intensity, and PCA was used for multivariate statistics and visualization, specifically for outlier detection.

From the MS-DIAL results file, all detected features/metabolites were removed if (sample max)/(blank average) < 10. Known (positively identified/annotated) features/metabolites were evaluated for MSI level 1 matches [33]. Next, positive and negative mode data were combined and replicate identifications removed by initially retaining features with an MSI level 1 match. Because MS-DIAL does not evaluate MS/MS data for metabolites with both m/z and retention time matches, manual evaluation of spectra was performed to confirm level 1 identifications. Manual inspection of spectra for MSI level 2 matches was conducted in specific cases flagged by parameters requiring further investigation. Remaining replicate features without an MSI level 1 match were filtered by retaining those with the highest MS-DIAL total score. Detected synthetic drugs were removed from the dataset because they were not relevant to metabolite changes in response

to the experimental treatment. For all features not positively identified (unknowns), after removal based on the above sample max/blank average threshold, unknowns with both m/z and MS2 data were retained and are reported separately. All sample peak heights (semi-quantitative) were normalized to the metabolite total ion chromatogram (mTIC) for each analysis (RPLC–positive, RPLC–negative). To perform statistical analyses, processed peak intensity data above the 100,000 threshold for compound detection from the *U. cynodontis*, Tulsi callus, and co-culture samples were uploaded to MetaboAnalyst 6.0 [34]. Peak intensity data were log-transformed, and MetaboAnalyst was used to generate PCA plots and heatmaps to describe unique metabolomic profiles among the sample groups.

2.5. Identification of Metabolites with Antioxidative and Anti-Inflammatory Properties

To investigate whether metabolites identified by untargeted metabolomics have antioxidative or anti-inflammatory properties, we used the annotation pipeline described in Zemach et al. [30]. Briefly, these known metabolites were searched against the PubMed database to discover abstracts that support whether they have antioxidative or anti-inflammatory properties. Specifically, we searched using the phrase ({metabolite}[TIAB] AND (antiox* OR anti-ox*)[TIAB]) to find abstracts that had both the metabolite and any antioxidant name derivative in either the title and/or abstract. We then searched the phrase ({metabolite}[TIAB] AND (anti-inflamma*, antiinflamma*, OR inflammat*)TIAB]) to find anti-inflammatory related papers. Titles and abstracts were downloaded from papers that matched this search and subsequently filtered to remove non-matching metabolite entries. Abstracts were excluded if the text contained target metabolite name mismatches or partial matches.

The filtered title and abstract text data were used as input for text annotation using OpenAI's large language model GPT-4.1 mini (ChatGPT, see Table S1 for prompt information). The ChatGPT answers were downloaded, and a subset of annotations were cross verified manually for accuracy. GPT and manual annotation data were imported into R to determine how accurate ChatGPT was in annotating titles and abstracts for metabolites having antioxidant and anti-inflammatory activity. To assess this model, we determined the probability that a certain number of "Yes" by GPT would correctly correspond to human annotations. Metabolites were grouped into categories based on the number of GPT "Yes" annotations. For each category, ranging from 1 to 10 "Yes" annotations, four metabolites were randomly sampled. Each sample dataset consisted of 220 papers representing 40 different metabolites.

For each "Yes" count threshold (1–10 "Yes"), the probability was calculated for correct identification by GPT. There had to be at least one "Yes" manual annotation that matched a GPT "Yes" annotation to be labeled as correct. The probability was calculated as the ratio of correct identifications (metabolites with at least one "Yes" manual annotation) to the total number of selected metabolites. This ratio represents the likelihood that a GPT annotation is correct when it meets or exceeds the given threshold:

$$\text{Probability} = \frac{\text{Number of correclty identified metabolites}}{\text{Total number of selected metabolites}}$$

where the numerator, the number of correctly identified metabolites, is greater than or equal to one "Yes" manual annotation and the denominator, the total number of selected metabolites, is the total number of metabolites that meet or exceed the specified GPT "Yes" threshold. This process was then repeated for a total of 10,000 times using different randomly sampled pools of metabolite and paper samples, and the mean probability and standard deviation were calculated.

2.6. 2,2-Diphenyl-1-Picrylhydrazyl (DPPH) Radical Scavenging Assay

The radical scavenging activity was quantified using the DPPH assay [35]. Conditioned media and the uncultivated culture-medium control (0.1 mL) were mixed with 0.9 mL of 81 µM DPPH in methanol and incubated in the dark at room temperature for 1 h. Absorbance was measured at 517 nm using a BioTek Synergy LX spectrophotometer (Winooski, VT, USA). Measurements were performed on three biological replicates. Results were expressed in micromolar equivalents of vitamin C (L-ascorbic acid), which was calibrated using concentrations from 0 to 500 µM.

2.7. Intra-Cellular ROS Activity Assay

Intracellular ROS levels were determined by measuring DCF fluorescence intensity. Human dermal fibroblasts (HF), previously established in our laboratory [36], were maintained in serum-free medium (SFM) supplemented with 10% human fibroblast-conditioned medium (HF-CM) and 2% human serum (HS). Cells were plated at 1×10^4 per well in a 96-well plate and allowed to attach overnight at 37 °C with 5% CO_2. The cells were then washed and treated with DMEMF12 + 1% HS as control medium, 1% Tulsi, 1% Ustilago, or 1% Ustilago-Tulsi (CFx-α1) for 2 h. Three biological replicates were plated for each treatment condition using biologically replicated Tulsi, Ustilago, and CFx-α1 media. After treatment, the cells were washed with PBS and stained with 10 µM H2DCFDA (BLD Pharmatech, Cincinatti, OH, USA) for 30 min at 37 °C in the dark. The cells were then washed once, and fresh PBS was added. Fluorescence was read immediately using a Biotek Synergy LX multi-mode reader (Winooski, VT, USA) with excitation and emission wavelengths of 485 nm and 528 nm, respectively. Relative ROS levels were calculated by normalizing the fluorescence intensity of treated cells to that of control cells.

2.8. Lipopolysaccharide (LPS) Induced Inflammation Assay

Human microvascular endothelial cells-1 (HMEC-1; ATCC CRL-3243) were selected as a skin-relevant inflammatory model because dermal microvascular endothelial cells participate in cutaneous inflammatory signaling and exhibit NF-κB activation in response to inflammatory stimuli [37–39]. Cells were cultured in MCDB131 medium without L-glutamine (Life Technologies, Carlsbad, CA, USA), supplemented with 10 ng/mL epidermal growth factor (EGF; Thermo Fisher Scientific), 1 µg/mL hydrocortisone (Sigma, Carlsbad, CA, USA), 10 mM glutamine (ATCC 30-2214), and fetal bovine serum (FBS; ATCC 30-2020). Cells were plated on collagen-coated coverslips (Electron Microscopy Sciences, Hatfield, PA, USA) at a density of 2.5×10^4 cells/well and incubated for 7 days until confluency. Cells were then washed and treated for 1 h with control medium (negative control), 5 µg/mL LPS (Sigma; positive inflammatory control), LPS + 1% Tulsi, LPS + 1% Ustilago, or LPS + 1% Ustilago–Tulsi (CFx-α1). The 1-h time point was selected because LPS-induced NF-κB nuclear translocation in HMEC-1 cells occurs rapidly and is strongly detectable within 30–60 min [36,40]. Three biological replicates were plated for each treatment condition using biologically replicated Tulsi, Ustilago, and CFx-α1 media. After incubation, cells were fixed with 4% paraformaldehyde (Santa Cruz Biotechnology, Dallas, TX, USA) for 20 min and permeabilized with 0.3% Triton X-100 (Sigma) for 5 min. Coverslips were blocked with Superior™ Blocking Buffer (G-Biosciences, St. Louis, MO, USA) for 1 h with gentle rocking, then incubated with anti-NF-κB p65 antibody (Abcam, Waltham, MA, USA) overnight at 4 °C. Coverslips were washed three times with 1× PBS for 10 min each and incubated with goat anti-rabbit IgG (H + L) highly cross-adsorbed secondary antibody, Alexa Fluor™ Plus 555 (Thermo Fisher Scientific), for 1 h at room temperature in the dark with gentle rocking. Coverslips were washed again and mounted on slides using VECTASHIELD® Vibrance™ Antifade Mounting Medium with DAPI (Vector Laboratories, Newark, CA, USA). Slides

were imaged and analyzed using ImageJ software version 1.54p (NIH, Bethesda, MD, USA). The inflammatory response was quantified by counting NF-κB p65-positive nuclei, defined by pink nuclear staining, and dividing this number by the total number of DAPI-stained nuclei. The result was multiplied by 100 to obtain the percentage of inflammatory cells.

2.9. Cell Viability Assay

The same human dermal fibroblasts (HF) and culture conditions described in Section 2.7 were used for the cell viability assay. Cells were treated with 1%, 3%, or 5% unconditioned MS culture medium, Tulsi (T)-conditioned medium, *Ustilago* (U)-conditioned medium, or CFx-α1. Untreated cells served as the control. After 24 h, cell viability was assessed using the MTS [3-(4,5-dimethylthiazol-2-yl)-5-(3-carboxymethoxyphenyl)-2-(4-sulfophenyl)-2H-tetrazolium] assay (CellTiter 96® AQueous One Solution Cell Proliferation Assay, G3582; Promega, Madison, WI, USA) according to the manufacturer's instructions. MTS reagent (20 µL) was added to 100 µL of culture medium per well and incubated for 4 h before absorbance was measured at 490 nm using a BioTek Synergy LX plate reader. Background absorbance from medium-only wells was subtracted from each measurement, and cell viability was normalized to untreated cells. Measurements were performed in triplicate (n = 3).

2.10. GenAI Disclosure

During preparation of this work, the authors used OpenAI's GenAI model to assist with literature screening and classification. The model evaluated PubMed titles and abstracts to determine whether publications reported direct experimental evidence supporting the antioxidant or anti-inflammatory activity of metabolites of interest. Its classifications contributed to the literature-based metabolite annotations. A subset of the classifications was manually reviewed, and annotation accuracy was evaluated as described in Section 2.5. The model was not used to generate experimental data or perform statistical analyses. The authors reviewed and validated the outputs and take full responsibility for the content of the publication.

3. Results

3.1. Development and Genome Sequencing of Ustilago and Tulsi Cell Cultures

Tulsi cell culture was established from an *O. sanctum* plant (Figure 1a). *U. cynodontis* was isolated from a local bermudagrass plant (Figure 1a). Species identification of the Ustilago culture was performed by ITS sequencing (Figure S1A,B). To further investigate the relationship of this Ustilago strain to other Ustilaginaceae species, its genome was sequenced and compared with 12 other Ustilaginaceae genomes. A phylogenetic tree based on genomic sequencing clustered this Ustilago strain together with the reference *U. cynodontis* genome, confirming its species identity (Figure 1b). Further analysis of the genome of this *U. cynodontis* strain identified 16,694 genetic variants relative to the published *U. cynodontis* genome (Figure S1C). Genetic variants were relatively enriched in repeat regions and depleted in gene-coding sequences (Figure S1C). In genic exons, the genetic variant frequency was approximately 3 per 10 kb, whereas in repeat sequences it was closer to 23 per 10 kb, about sevenfold higher (Figure S1C).

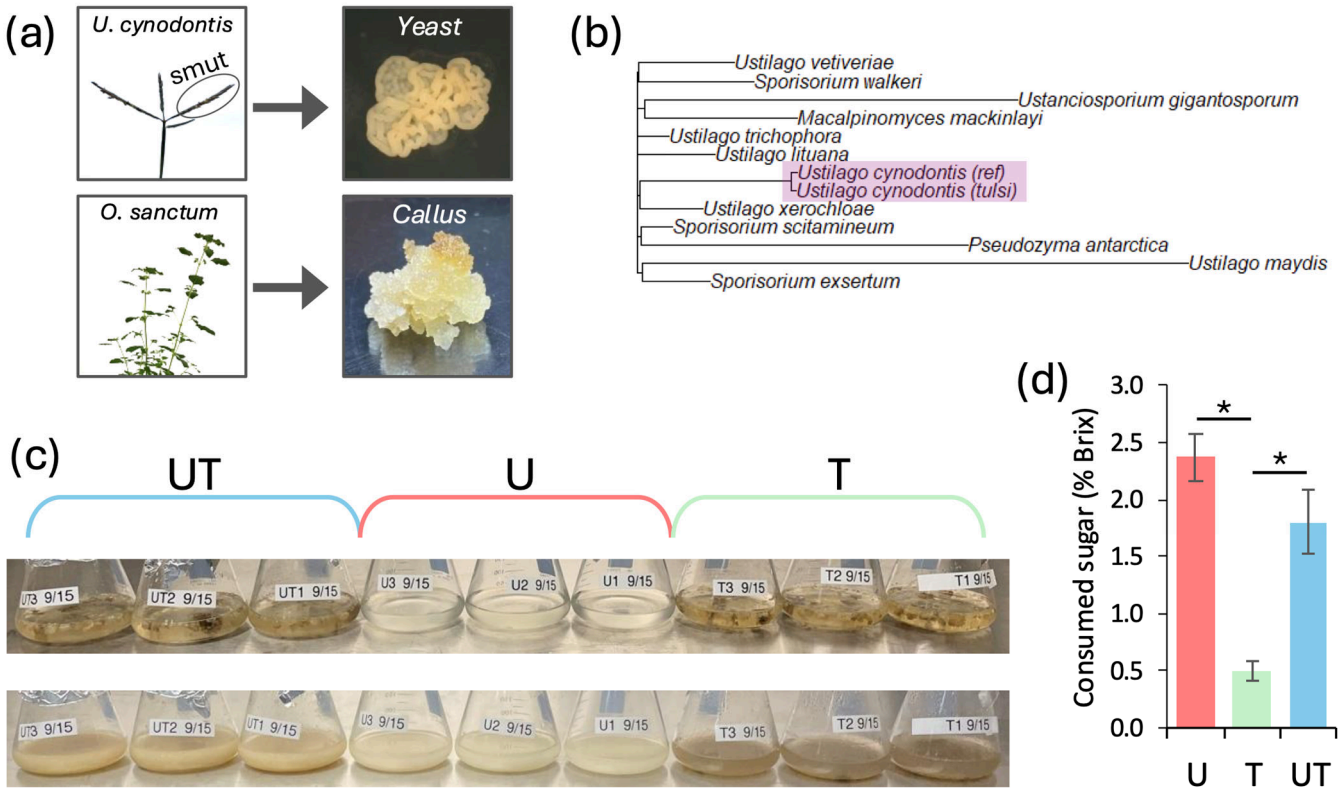


Figure 1. Development of the Ustilago–Tulsi co-culture system. (**a**) Isolation of *Ustilago cynodontis* from a Bermudagrass plant (**top**), and the development of Tulsi cell culture (**bottom**). (**b**) A phylogenetic tree based on the genomes of 12 Ustilaginaceae species and the one isolated in this study, *U. cyndontis* reference and our strain (tulsi) highlighted in purple. (**c**) Tulsi (T), Ustilago (U), and Ustilago-Tulsi (UT) cultures at induction (**top**) and at harvest (**bottom**). (**d**) Average sugar consumption at harvest (*, Student's *t*-test $p < 0.005$). Error bars represent standard deviation (SD).

3.2. CFx-α1 Unique Metabolome

Ustilago (U) and Tulsi (T) cells from callus were cultivated in flasks either separately or together (UT, Ustilago–Tulsi co-culture) (Figure 1c). At the 7-day harvest point, sugar consumption in the Ustilago–Tulsi co-culture was slightly lower than in the Ustilago monoculture, although the difference was not statistically significant, whereas both Ustilago-containing cultures consumed significantly more sugar than the Tulsi monoculture (Figure 1d). Harvested cultures were centrifuged, and their corresponding media were subjected to untargeted metabolomics by LC–MS (Table S2). The metabolites sucrose, pyridoxine, thiamine, glycine, and biotin were present in our MS-media before inoculation and were detected by untargeted metabolomics and subsequently removed. Principal component analysis (PCA), hierarchical clustering, and Pearson correlation of the identified metabolite profiles separated the plant and yeast samples into distinct clusters (Figure 2a–c). The UT co-culture metabolomes, termed CFx-α1, formed a distinct cluster from either of the single cultures, while clustering more closely with the Ustilago samples than with the Tulsi samples (Figure 2a–c). In addition, the CFx-α1 metabolite profile was distinct from the simple sum of the single cultures (U + T), indicating that the CFx-α1 differs from a mere mixture of single-culture secretomes (Figure 2d). Overall, these results indicate that the CFx-α1 secretome is unique and distinct from the secretomes of the single cultures, either separately or mixed post-harvest.

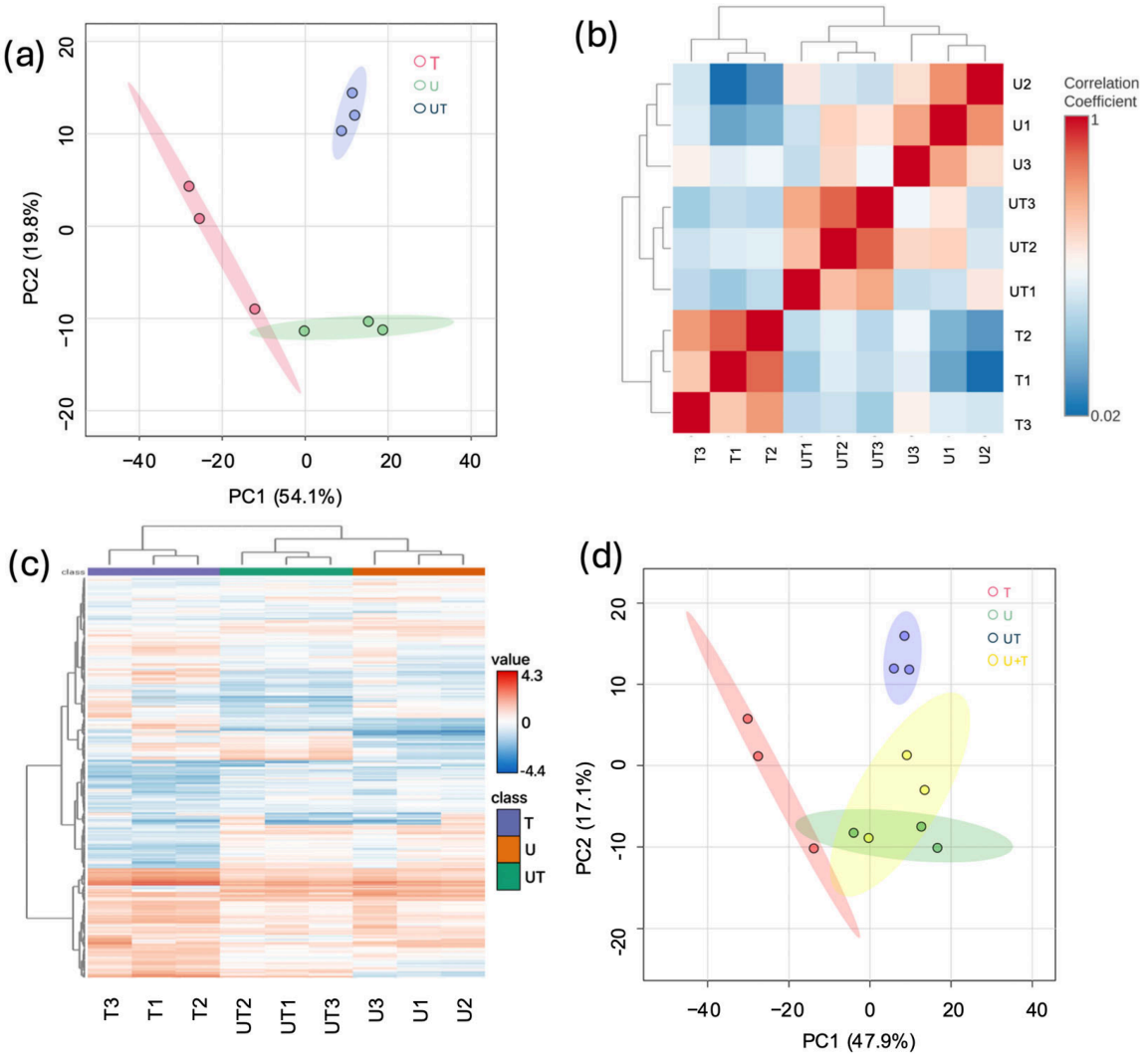


Figure 2. CFx-α1 unique metabolome. (**a**–**c**) Clustering of LC-MS intensity (median normalized and log transformed) of identified metabolites (MSI1 and MSI2) from three biological replicates of each culture as principal component analysis (PCA) (**a**), Pearson correlation clustering (**b**), and Euclidean distance with Ward's linkage hierarchical clustering (**c**). U, T, and UT stand for Ustilago, Tulsi, and Ustilago-Tulsi (CFx-α1), respectively. (**d**) PCA as in A, including in-silico simulated U + T profiles generated from the two monocultures.

3.3. CFx-α1 Enriched Metabolome

Next, metabolites that were differentially regulated in the CFx-α1 compared with the secretomes of U or T cultured individually were identified (Figure 3a). This analysis revealed that the CFx-α1 is relatively enriched in metabolites compared with secretomes derived from single cultures. Notably, this metabolite enrichment was not accompanied by greater sugar consumption, as the Ustilago–Tulsi co-culture consumed a similar amount of sugar to the Ustilago monoculture at harvest (Figure 1d). Among the differentially regulated metabolites (DRMs), more metabolites were upregulated in CFx-α1 than in either of the single cultures (Figure 3b). CFx-α1 contained 429 and 163 upregulated DRMs (up-DRMs) relative to Tulsi and Ustilago, respectively, which is approximately fourfold and twofold higher than the corresponding numbers of downregulated DRMs (down-DRMs) in CFx-α1 versus T (98) and U (80). Additionally, the relative fold change of CFx-α1 up-DRMs was two- to threefold higher than that of down-DRMs (Figure 3b). Specifically, the average log2 fold change of CFx-α1 up-DRMs versus T and U was 7.1 and 5.3, respectively, whereas the corresponding down-DRMs displayed average log2 fold changes of −3.4 and

−1.7 (Figure 3b). Next, we compared the overlap between upregulated DRMs in CFx-α1 versus U and CFx-α1 versus T, as well as between the corresponding downregulated DRMs (Figure 3c). Of the 429 metabolites upregulated relative to T and 163 upregulated relative to U, 89 were shared between the two sets. A hypergeometric test was used to determine whether this overlap was greater than expected by chance, using the 1473 unique identified metabolites in the dataset as the background population. The null hypothesis was that membership in the two upregulated DRM sets was independent. The observed overlap was approximately twofold greater than expected by chance and was statistically significant ($p = 3.891 \times 10^{-13}$). In comparison, eight metabolites were mutually downregulated, representing a 1.5-fold enrichment that was not statistically significant ($p > 0.05$). No enrichment was observed between other DRM combinations, i.e., upregulated versus downregulated DRMs in either direction (Figure S2A,B). These results suggest that the CFx-α1 is enriched in metabolites compared with either of the single cultures and that the set of mutually upregulated metabolites is non-random.

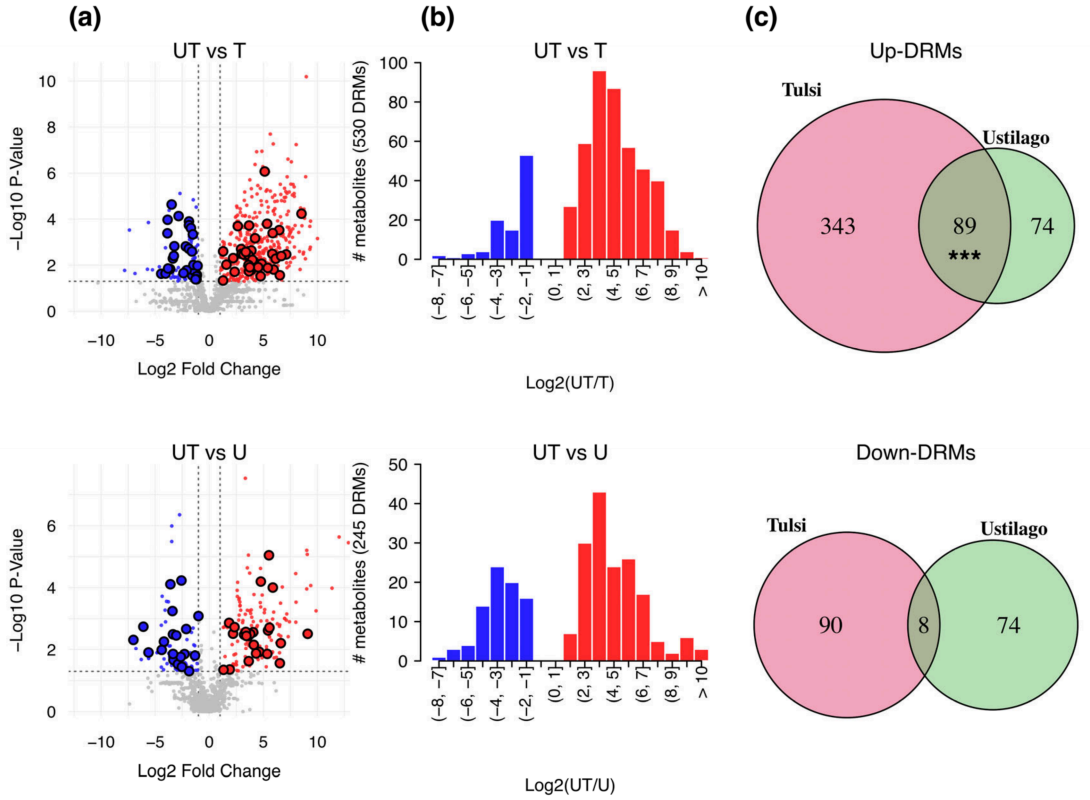


Figure 3. CFx-α1 enriched metabolome. (**a**) Volcano plots of metabolites in Ustilago-Tulsi over the single Tulsi (**top**) or Ustilago (**bottom**). Up and down differentially regulated metabolites (DRMs) were highlighted with red and blue, respectively. Bolded circles mark antioxidant metabolites (see Figure 4a). (**b**) Distribution of DRMs across Log2 fold change of LC-MS intensity in Ustilago-Tulsi over the single Tulsi (**top**) or Ustilago (**bottom**). (**c**) Overlap between upregulated (**top**) and downregulated (**bottom**) DRMs shown in panels (**a**,**b**). The 89 mutually upregulated DRMs were enriched approximately twofold above that expected by chance (hypergeometric test, $p = 3.891 \times 10^{-13}$). U, T, and UT stand for Ustilago, Tulsi, and Ustilago-Tulsi (CFx-α1), respectively. *** $p < 0.001$.

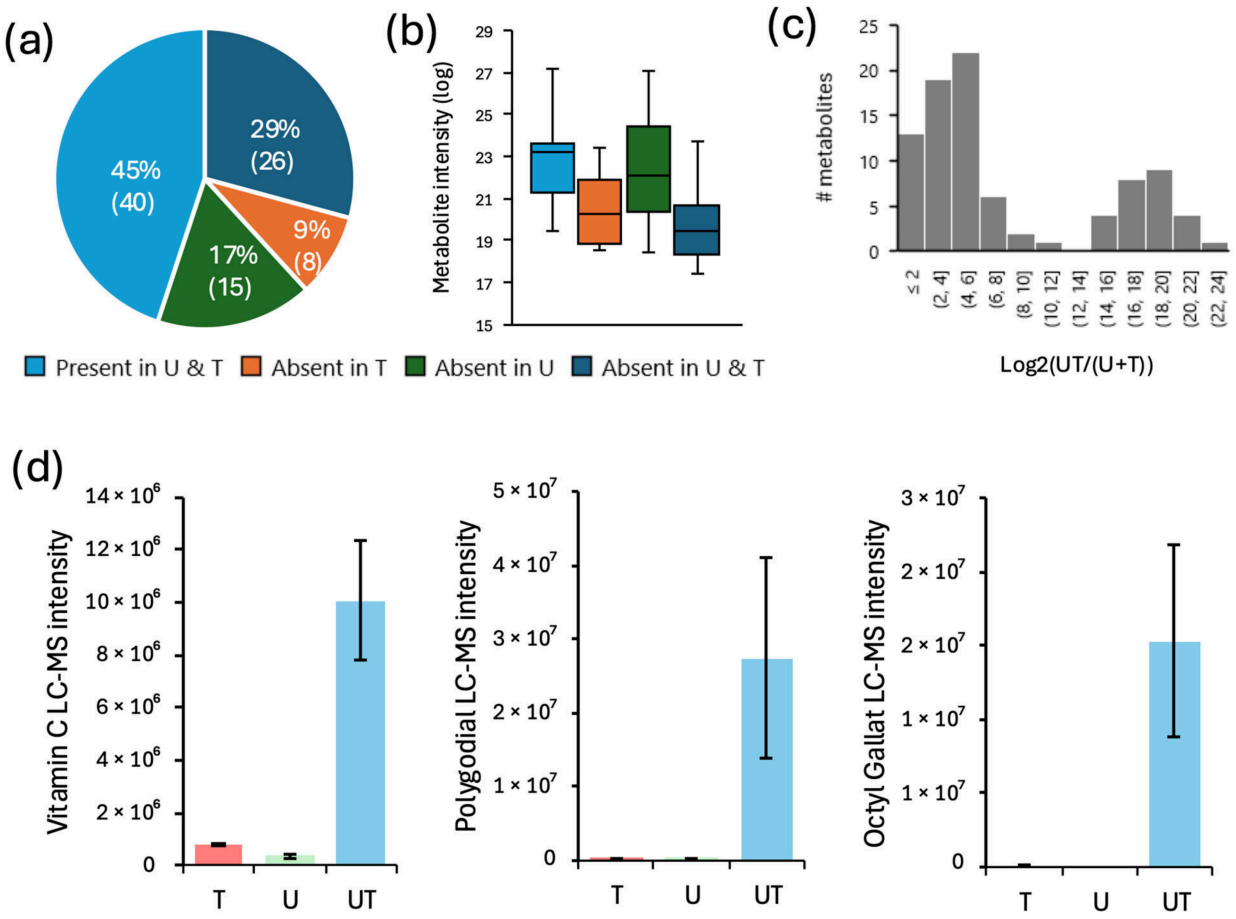


Figure 4. Synergistic upregulation of beneficial metabolites in the CFx-α1 metabolome. (**a**) Proportions of the different categories of mutually upregulated DRMs in the Ustilago-Tulsi metabolome, i.e., those that were upregulated in UT over U and T. (**b**) Log intensity of metabolites in UT separated into four groups based on their presence status in the single cultures. (**c**) Distribution of mutually upregulated DRMs in UT versus single cultures across Log2-fold change in metabolite intensity in UT versus the sum of single cultures. (**d**) Metabolite LC-MS intensity of upregulated metabolites in UT that were present in U and T (Vitamin C), present only in one of the cultures (polygodial), or absent in both single cultures (octyl gallate). Error bars represent SD. LC-MS analyses were based on $n = 3$ biological replicates per culture. U, T, and UT stand for Ustilago, Tulsi, and Ustilago-Tulsi (CFx-α1), respectively.

3.4. Synergistic Upregulation of Beneficial Metabolites in the CFx-α1 Metabolome

To further investigate the nature of mutually upregulated metabolites in CFx-α1 compared with single cultures, these metabolites were classified into four categories based on their presence in the single cultures: (1) metabolites present in both single cultures, (2) metabolites present in U but absent in T, (3) metabolites present in T but absent in U, and (4) metabolites absent from both U and T (Figure 4a). Metabolite intensity in CFx-α1 differed among the four groups, with the highest and lowest median intensities observed in the groups of metabolites present in both single cultures and absent from both single cultures, respectively (Figure 4b). The largest group with 40 mutually upregulated metabolites (45%) was the one with metabolites found in both single cultures (Figure 4a). Twenty-three metabolites, accounting for 26% of mutually upregulated metabolites, were found in only one of the single cultures (Figure 4a). Notably, a substantial fraction (29%) of the mutually upregulated metabolites in CFx-α1 belonged to the group that was absent from both single cultures (Figure 4a), suggesting de novo synthesis in the CFx-α1 metabolome. In addition, 85% of the mutually upregulated metabolites were enriched by at least fourfold

in the CFx-α1 sample compared with the combined single cultures (U + T), implying a potent synergistic upregulation in CFx-α1 (Figure 4c). Vitamin C, polygodial, and octyl gallate are examples of metabolites from three different categories that were synergistically upregulated in CFx-α1 (Figure 4d). These metabolites have been reported to possess antioxidant, anti-inflammatory, antimicrobial, or wound-healing properties [41–43], suggesting potential health benefits of CFx-α1.

3.5. CFx-α1 Is Enriched in Antioxidant Metabolites and Exhibits Corresponding Activity

Observing the activation of Vitamin C in the CFx-α1 metabolome, we next aimed to profile the general activation of antioxidant metabolites in each of the cultures. To do so, we developed an algorithm to annotate metabolites as antioxidants based on scientific publications (Figure 5a). The first step in the annotation process is searching for metabolites on PubMed. Here, we used the 1473 metabolites identified by the untargeted metabolomics data. Out of the total metabolites, 859 of them have been mentioned in papers, either in the title or abstract, along with the 'antioxid*' term. For accuracy, we excluded papers with a partial match to our metabolite (i.e., modified metabolites), leaving us with 353 metabolites. In the next step, we ran the title and abstract through the GPT model to inquire about the direct role of the metabolite in antioxidation, which resulted in 243 metabolites. Manual review suggested 95% accuracy of the GPT classification for metabolites with at least one positive/antioxidant classified paper (Figure 5b). The GPT success rate gradually increased with the number of positive classifications, reaching 100% for metabolites with at least five positive antioxidant classification, concluding 101 metabolites (Figure 5a).

Focusing on the 101 annotated antioxidant metabolites, we found that CFx-α1 contained more antioxidants than either of the single cultures, i.e., 38 antioxidants compared to 32 for either U or T. Additionally, substantially more antioxidants were differentially upregulated than downregulated in CFx-α1 compared to either of the single cultures, specifically two times more in CFx-α1 versus U and five times more in CFx-α1 versus T (Figure 5b). Furthermore, quantification of LC-MS intensity showed antioxidants in CFx-α1 to be significantly more abundant than in the single cultures (Figure 5c,d). Antioxidants can exhibit a range of antioxidation potency. Therefore, we next normalized the abundance of antioxidants to their averaged published activity level and still found that the CFx-α1 samples had a higher total abundance of antioxidants than either of the single cultures (Figure 5e). Finally, we tested the antioxidant potency of the different samples using the DPPH radical scavenging assay [35], including the uncultivated culture medium as a control. Neither the uncultivated medium nor Tulsi showed detectable DPPH radical-scavenging activity. Ustilago showed significantly greater activity than Tulsi, while CFx-α1 exhibited the highest activity and was significantly greater than both single cultures (Figure 5f). Next, we tested the effect of the conditioned media samples on the level of intracellular reactive oxygen species (ROS) in live human dermal fibroblasts (HF) cells. HF cells were pre-incubated for 2 h with 1% of T, U, or CFx-α1 conditioned media, followed by staining with 2′,7′-dichlorodihydrofluorescein diacetate (DCFDA). Fluorescent analysis found cells treated with CFx-α1 had intracellular ROS levels lower than either single culture, and 63% lower levels than control cells (t-test, $p < 0.0327$) (Figure 5g). Overall, these results suggest a robust and synergistic antioxidant potency of the CFx-α1 compared to the single cultures.

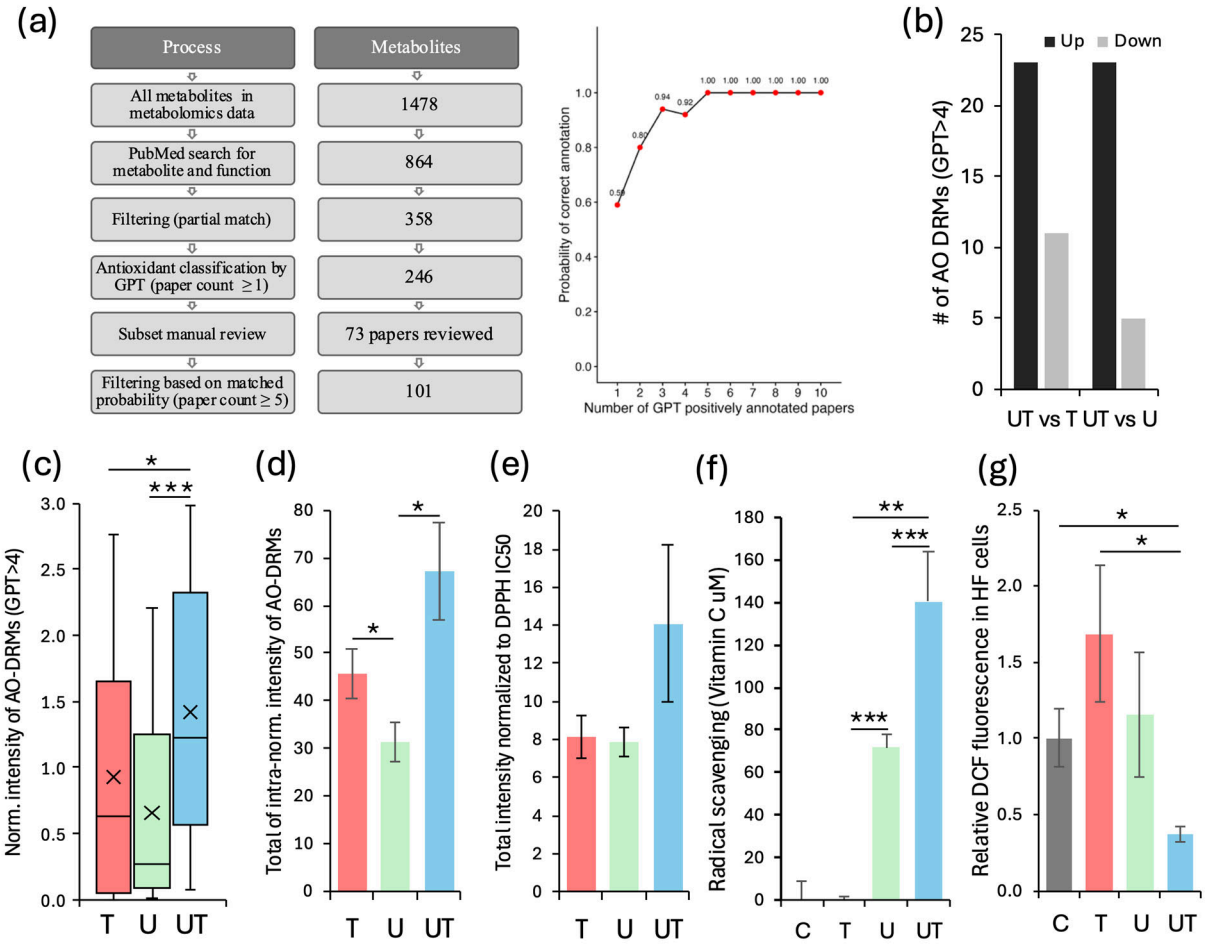


Figure 5. CFx-α1 is enriched in antioxidant metabolites and exhibits enhanced antioxidant activity. (**a**) Flowchart for the annotation of metabolites as antioxidants based on scientific publications (**left**) and antioxidant annotation accuracy as a function of the number of positive publications (**right**). (**b**) Number of up- and downregulated antioxidant (AO) DRMs (supported by ≥5 publications). (**c**) Boxplot of normalized intensities of antioxidant metabolites. (**d**) Combined normalized intensity of antioxidant metabolites. (**e**) Total intensity of antioxidant metabolites normalized within metabolites and by their reported DPPH IC50 values. (**f**) DPPH radical-scavenging activity of the base culture medium control—C and conditioned media from T, U, and UT cultures, expressed as vitamin C equivalents. (**g**) DCF fluorescence intensity in human dermal fibroblast (HF) cells treated with T, U, or UT conditioned media relative to untreated control cells—C. Where applicable, values represent the mean ± SD of three biological replicates. T, U, and UT denote Tulsi, *Ustilago*, and *Ustilago*–Tulsi (CFx-α1), respectively. *, **, and *** denote *t*-test, $p < 0.05$, $p < 0.01$, and $p < 0.001$, respectively.

3.6. CFx-α1 Is Enriched in Anti-Inflammatory Metabolites and Exhibits Corresponding Activity

Oxidative stress and chronic inflammation are interconnected processes that can form a destructive, self-amplifying cycle in the body [44]. Excess ROS damages cells and activates the redox-sensitive transcription factor NF-κB [45,46]. Once activated, NF-κB regulates the production of inflammatory cytokines [47]. To investigate the anti-inflammatory potential of the U, T, and CFx-α1 samples, we first identified anti-inflammatory metabolites in their extracellular metabolomes.

Of the 1473 metabolites identified in this study, 847 were mentioned in the titles or abstracts of publications containing the terms "anti-inflamma*," "antiinflamma*," or "inflammat*". For accuracy, we excluded papers containing only partial matches to the identified metabolites (i.e., modified metabolites), leaving 409 metabolites for further analysis. In the next step, we evaluated the titles and abstracts using a GPT model to determine

whether they described a direct role for each metabolite in inflammation, resulting in 171 candidate metabolites. Manual review of 209 of the 243 positively annotated papers confirmed the accuracy of the GPT classification for metabolites supported by at least two papers positively classified for anti-inflammatory activity, resulting in the identification of 112 anti-inflammatory metabolites (Figure 6a).

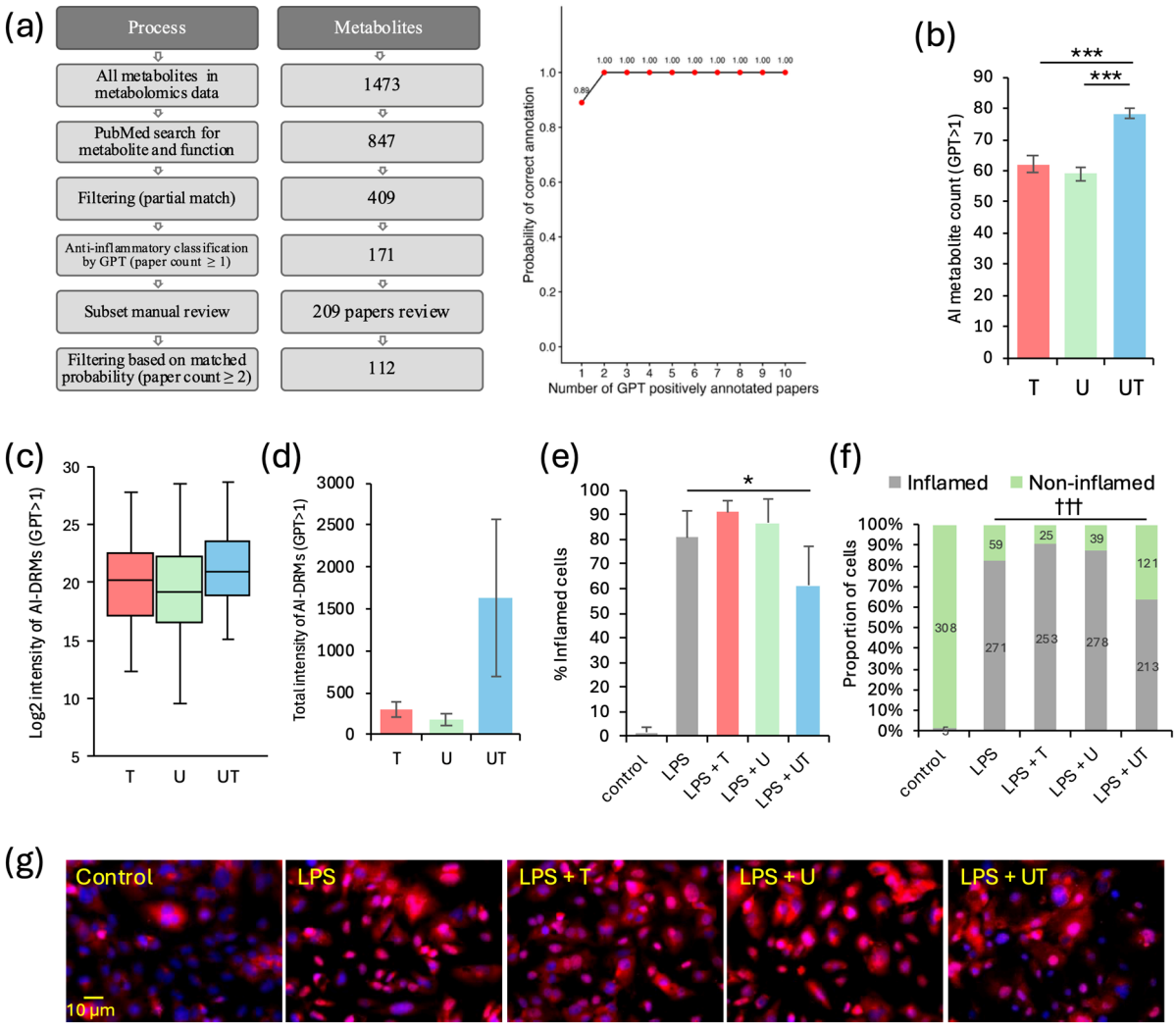


Figure 6. CFx-α1 is enriched in anti-inflammatory metabolites and exhibits corresponding activity. (**a**) A flowchart for the annotation of metabolites as anti-inflammatory from scientific publications (**left**). Annotation accuracy of anti-inflammatory increases with the number of positive publications (**right**). (**b**) Number of differentially regulated anti-inflammatory metabolites detected in the indicated samples. (**c**) Boxplot of normalized intensities (per-metabolite) of anti-inflammatory metabolites. (**d**) Combined intensity of anti-inflammatory metabolites. (**e**) Percent red (inflamed) nuclei of HMEC-1 cells not treated (control) or treated with LPS with or without 1% of U, T, or CFx-α1. (**f**) Proportions of inflamed and non-inflamed HMEC-1 cells. (**g**) Representative fluorescent images of HMEC-1 cells stained with DAPI (blue) and immuno-stained for NF-κB (red). Metabolomic analyses in panels b-d were based on $n = 3$ biological replicates per culture. Cellular analyses in panels e-g were performed with $n = 3$ biological replicates. Error bars, where shown, represent SD. *, and *** denote *t*-test $p < 0.05$, and $p < 0.001$, respectively; ††† denotes Fisher's exact test $p < 1.0 \times 10^{-6}$.

Among these 112 annotated anti-inflammatory metabolites, 85 were identified as DRMs. Focusing on these 85 metabolites, we found that CFx-α1 contained more anti-inflammatory metabolites than either single culture, with 78 metabolites compared with 62 and 59 in the T and U cultures, respectively (Figure 6b). Additionally, quantification of

LC–MS intensities showed that the anti-inflammatory metabolites in CFx-α1 were more abundant than in the single cultures (Figure 6c,d). Notably, several metabolites annotated with both antioxidant and anti-inflammatory activities were strongly enriched in CFx-α1, including octyl gallate, rosmarinate, costunolide, atractylenolide III, verminoside, and esculin (Figure S3). To evaluate the anti-inflammatory potential of the samples, we assessed their effects on lipopolysaccharide (LPS)-induced NF-κB nuclear localization in human dermal microvascular endothelial cells (HMEC-1). Among the three samples, only CFx-α1 significantly reduced LPS-induced NF-κB nuclear localization by 25% (*t*-test $p < 0.05$; Fisher's exact test $p < 1.0 \times 10^{-6}$) (Figure 6e–g). These results indicate that CFx-α1 is enriched in anti-inflammatory metabolites and exhibits corresponding activity in human skin-derived cells.

3.7. CFx-α1 Maintains Fibroblast Metabolic Activity Across Increasing Concentrations

To further evaluate the biocompatibility of CFx-α1, human dermal fibroblasts were treated with increasing concentrations (1%, 3%, and 5%) of unconditioned MS culture medium, monoculture-conditioned media, or CFx-α1, and cellular metabolic activity was assessed using the MTS assay (Figure 7). At 1%, MTS activity remained between 88% and 99% of the untreated control for the three conditioned media, with no significant differences from untreated cells (*t*-test, $p > 0.05$). At 3%, CFx-α1 maintained an MTS signal at 111% of the untreated control, compared with 82%, 74%, and 88% for MS medium, Tulsi, and *Ustilago*, respectively; none of these differences reached statistical significance relative to the untreated control.

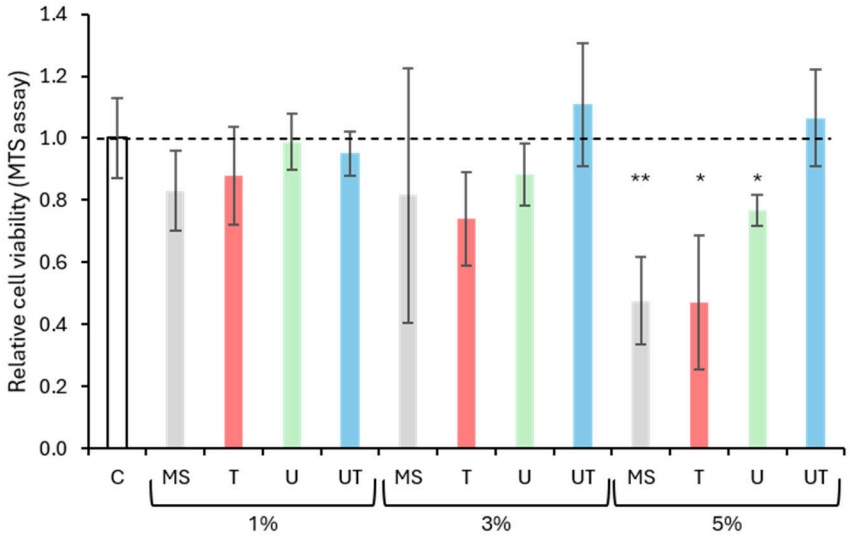


Figure 7. CFx-α1 maintains human dermal fibroblast metabolic activity across increasing concentrations. Human dermal fibroblasts (HF) were treated with 1%, 3%, or 5% unconditioned MS culture medium (MS), T, U, or CFx-α1. Untreated cells served as the control. Cellular metabolic activity was measured using the MTS assay and normalized to untreated cells. Bars represent mean ± SD ($n = 3$). The dotted line represents the relative cell viability of the control sample (C, 1.0). Statistical comparisons were made against untreated cells using a *t*-test, $p < 0.05$ (*) and $p < 0.01$ (**).

At 5%, the effect of the treatments became more pronounced. Unconditioned MS medium reduced the MTS signal to 48% of the untreated control ($p = 0.0089$), while Tulsi and *Ustilago* conditioned media resulted in 47% ($p = 0.0215$) and 77% ($p = 0.0429$), respectively. In contrast, CFx-α1 maintained the MTS signal at 107% of the untreated control and was not significantly different from untreated cells ($p = 0.607$). Thus, CFx-α1 maintained fibroblast metabolic activity across the tested concentration range, including at 5%, where

the unconditioned medium and both monoculture conditioned media showed reduced MTS signals.

4. Discussion

Our study demonstrates that the yeast–plant-derived Consortia Factors preparation CFx-α1 exhibits a markedly enriched and distinct extracellular metabolomic profile compared with the corresponding monoculture conditioned media, underscoring the capacity of this biologically driven plant–microbial consortium to increase the relative abundance of bioactive compounds beyond that observed in either monoculture. Metabolomic analysis revealed enrichment of antioxidants, organic acids, and other bioactive metabolites in CFx-α1, suggesting metabolic interplay between the partners.

One particularly striking observation was the increased relative abundance of vitamin C in CFx-α1. While vitamin C was minimally detected in both monocultures, its LC–MS intensity in CFx-α1 was 13-fold higher than in Tulsi and 27-fold higher than in Ustilago. This suggests that the co-culture environment alters metabolic processes affecting vitamin C production or accumulation. Possible mechanisms include precursor cross-feeding, stress-induced signaling, and activation of plant defense pathways, all of which may stimulate antioxidant biosynthesis [48,49].

Interestingly, this observation can be considered in the context of natural smut–host interactions. Huitlacoche, the edible corn smut caused by *Ustilago maydis*, has been reported to contain vitamin C and other nutrients [50]. The enrichment of vitamin C in CFx-α1 suggests that our cultivation process may share some features with natural interactions between smut fungi and their host plants, although the underlying mechanisms were not examined. This comparison provides ecological context for our approach and its potential biotechnological applications.

Beyond vitamin C, several metabolites strongly enriched in CFx-α1 were annotated with both antioxidant and anti-inflammatory activities, including octyl gallate, rosmarinate, costunolide, atractylenolide III, verminoside, and esculin (Figure S3). Several of these compounds showed only low signals in the monocultures but were markedly increased in CFx-α1, whereas costunolide and atractylenolide III were already present in both monocultures and were synergistically enriched under co-culture conditions. These compounds have been reported to act through mechanisms relevant to the cellular responses examined here. For example, rosmarinate, costunolide, and atractylenolide III have been associated with modulation of oxidative-stress responses and NF-κB-related inflammatory signaling, while esculin has been linked to antioxidant and NF-κB/MAPK pathways and verminoside to attenuation of LPS-induced inflammatory responses [51–55]. Octyl gallate has likewise been reported to exhibit antioxidant and anti-inflammatory activities [43]. These reported activities are consistent with the reduced intracellular ROS and attenuation of LPS-induced NF-κB nuclear localization observed with CFx-α1. Importantly, the aim of this study was not to assign the observed biological activities to individual metabolites. The Consortia Factors concept is based on the collective extracellular output of the co-culture, in which multiple co-culture-enriched metabolites may contribute together to the resulting biological activity. Accordingly, these compounds are best considered components of a broader functionally enriched metabolomic profile rather than as individual active ingredients responsible for the observed effects. Such co-culture-associated effects highlight the promise of consortium-based strategies for producing functional metabolites and offer a potential alternative to conventional single-organism fermentation systems [12,13].

Our finding that repeat regions in *U. cynodontis* contained genetic variants at a density of approximately 23 variants per 10 kb, nearly eight times the density observed in exonic regions (approximately 3 variants per 10 kb), is consistent with trends across fungi

and yeasts, in which repeat-rich compartments are hotspots for variation while coding sequences are highly conserved [56]. This supports the model of compartmentalized genome evolution, in which structural and regulatory diversity arises predominantly through repeat-associated variation while essential protein-coding functions are preserved. In our strain, such variation may contribute to regulatory diversity; however, its relationship to secondary metabolite production remains to be established. Because metabolomic profiling was performed only at the 7-day harvest point, future time-course studies will help define the dynamics and optimal harvest window of CFx-α1 metabolite production.

Biocompatibility testing further showed that CFx-α1 maintained fibroblast viability across concentrations of 1–5%. Notably, increasing concentrations of the unconditioned MS medium reduced cell viability, with a pronounced reduction at 5%, whereas CFx-α1 maintained viability comparable to untreated cells even at this concentration. The monoculture-conditioned media did not provide the same preservation at 5%, suggesting that the co-culture process modifies the extracellular composition in a manner that improves its compatibility with human fibroblasts. This finding is consistent with the central observation of this study that co-culture generates an extracellular metabolomic profile distinct from that of either monoculture and from a simple combination of the two monoculture secretomes.

The increased relative abundance of vitamin C and other metabolites associated with antioxidant and anti-inflammatory properties positions CFx-α1 as a potential source of bioactive compounds relevant for cosmetic applications. Consistent with its metabolomic profile, CFx-α1 demonstrated antioxidant activity and attenuated LPS-induced NF-κB nuclear localization in human skin-derived cells, supporting its anti-inflammatory potential. Oxidative stress and chronic inflammation are closely interconnected processes that contribute to skin aging, while disruption of skin-barrier homeostasis can further promote cutaneous inflammation [44,57,58]. Accordingly, the antioxidant activity and attenuation of inflammatory signaling observed for CFx-α1 support its potential relevance to cosmetic strategies aimed at mitigating aging-associated skin changes and maintaining skin-barrier homeostasis. Anti-inflammatory activity was assessed at a single concentration (1%); further dose–response and cytokine studies could provide additional characterization of CFx-α1. Vitamin C is a cornerstone of immune support, collagen synthesis, and skin health, making these findings particularly impactful for the development of functional foods, nutraceuticals, and cosmetics formulations.

5. Conclusions

Plant–yeast co-culture produced the Consortia Factors preparation CFx-α1, which exhibited a distinct extracellular metabolomic profile enriched in vitamin C and other metabolites associated with antioxidant and anti-inflammatory properties compared with the corresponding monoculture conditioned media. These metabolomic differences were accompanied by enhanced antioxidant activity and attenuation of LPS-induced NF-κB nuclear localization in human skin-derived cells, supporting the antioxidant activity and anti-inflammatory potential of CFx-α1. Together, these findings identify plant–yeast co-culture as a promising biotechnology platform for producing bioactive extracellular metabolites and support the further development of CFx-α1 as a biotechnology-derived cosmetic ingredient.

6. Patents

The work reported in this manuscript resulted in U.S. Patent No. 11,473,117 B2.

Supplementary Materials: The following supporting information can be downloaded at https://www.mdpi.com/article/10.3390/cosmetics13060290/s1, Figure S1: Genetic profiling of the Ustilago culture. (A) Blast analysis of ITS sequence of isolated fungus culture. (B) Homology of ITS sequencing between isolated fungus and *U. cynodontis*. (C) Number and frequency of genetic variants in the genome of this study; *U. cynodontis* strain vs. the reference *U. cynodontis* NBRC 9727 strain.; Figure S2: Overlaps between differentially regulated metabolites in UT vs. U or T. (A) Overlap between upregulated DRMs in UT vs. U (pink) and downregulated DRMs in UT vs. T (green). (B) Overlap between downregulated DRMs in UT vs. U (pink) and upregulated DRMs in UT vs. T (green). U, T, and UT stand for Ustilago, Tulsi, and Ustilago-Tulsi (CFx-α1), respectively. Figure S3: Synergistic upregulation of selected antioxidant and anti-inflammatory metabolites in CFx-α1. Metabolite LC–MS intensity of selected upregulated antioxidant and anti-inflammatory metabolites in Tulsi (T), Ustilago (U), and Ustilago–Tulsi co-culture (UT; CFx-α1). Bars represent the mean ± SD of three biological replicates. Table S1: GPT-4.1-mini prompts used to annotate downloaded PubMed title and abstract text data. Table S2: Untargeted metabolomics identified metabolites and peak intensity data.

Author Contributions: Conceptualization, A.Z. and N.N.; methodology, A.Z., N.N., M.R.P., D.S., M.P. and D.T.-A.; investigation, A.Z., M.R.P., B.S.L., M.P., D.S. and D.T.-A.; data curation, M.R.P. and A.Z.; formal analysis, M.R.P. and A.Z.; supervision, A.Z. and N.N.; writing—original draft preparation, A.Z., M.R.P. and N.N.; writing—review and editing, A.Z., M.R.P., D.T.-A. and N.N. All authors have read and agreed to the published version of the manuscript.

Funding: The research was funded by Rinati Labs.

Institutional Review Board Statement: Not applicable.

Informed Consent Statement: Not applicable.

Data Availability Statement: *U. cynodontis* genomic data have been deposited in National Center for Biotechnology Information (NCBI) under BioProject accession PRJNA1418748.

Acknowledgments: The authors would like to thank Elsa Torres and Victor Flores for their assistance with procurement and administrative support. During preparation of this work, the authors used OpenAI's GenAI model ChatGPT 4.1 mini to assist with literature screening and classification. The model was not used to generate experimental data or perform statistical analyses. The authors used ChatGPT 5.6 to generate Graphical Abstract. The authors reviewed and validated the outputs and take full responsibility for the content of the publication.

Conflicts of Interest: The authors are employees of Rinati Skin LLC, doing business as Rinati Labs. The authors declare that the research was conducted in the absence of any commercial or financial relationships that could be construed as a potential conflict of interest. Rinati Labs holds U.S. Patent No. 11,473,117 B2 and funded the preparation of this manuscript. The funder did not affect the experimental process and results in the study. The funding relationship does not affect the scientific quality of the manuscript.

Abbreviations

The following abbreviations are used in this manuscript:

CFx	Consortia Factors
CFx-α1	Ustilago-Tulsi consortia factors
DRM	Differentially regulated metabolite
Down-DRM	Downregulated differentially regulated metabolite
HF	Human dermal fibroblast
HMEC-1	Human dermal microvascular endothelial cell line 1
LPS	Lipopolysaccharide
NF-kB	Nuclear factor kappa B
ROS	Reactive oxygen species
T	Tulsi monoculture

U	Ustilago monoculture
Up-DRM	Upregulated differentially regulated metabolite
UT	Ustilago–Tulsi co-culture

References

1. Skalnikova, H.; Motlik, J.; Gadher, S.J.; Kovarova, H. Mapping of the Secretome of Primary Isolates of Mammalian Cells, Stem Cells and Derived Cell Lines. *Proteomics* **2011**, *11*, 691–708. [CrossRef] [PubMed]
2. Brown, K.J.; Seol, H.; Pillai, D.K.; Sankoorikal, B.J.; Formolo, C.A.; Mac, J.; Edwards, N.J.; Rose, M.C.; Hathout, Y. The Human Secretome Atlas Initiative: Implications in Health and Disease Conditions. *Biochim. Biophys. Acta Proteins Proteom.* **2013**, *1834*, 2454–2461. [CrossRef] [PubMed]
3. Caudy, A.A.; Mülleder, M.; Ralser, M. Metabolomics in Yeast. *Cold Spring Harb. Protoc.* **2017**, *2017*, 677–680. [CrossRef] [PubMed]
4. Bhukya, B.; Banoth, C.; Keshav, P.K.; Hussain, M.S.; Ajmera, S. Biotechnological Production of Various Fungal Metabolites and Their Applications in White Biotechnology. In *Sustainable Utilization of Fungi in Agriculture and Industry*; Bentham Science Publisher: Sharjah, United Arab Emirates, 2022; pp. 255–286.
5. Wu, T.; Kerbler, S.M.; Fernie, A.R.; Zhang, Y. Plant Cell Cultures as Heterologous Bio-Factories for Secondary Metabolite Production. *Plant Commun.* **2021**, *2*, 100235. [CrossRef] [PubMed]
6. Bapat, V.A.; Kavi Kishor, P.B.; Jalaja, N.; Jain, S.M.; Penna, S. Plant Cell Cultures: Biofactories for the Production of Bioactive Compounds. *Agronomy* **2023**, *13*, 858. [CrossRef]
7. Marchev, A.; Georgiev, M. Plant Cell Bioprocesses. In *Current Developments in Biotechnology and Bioengineering: Bioprocesses, Bioreactors and Controls*; Elsevier: Amsterdam, The Netherlands, 2017; pp. 73–95.
8. Sabater-Jara, A.B.; Almagro, L.; Belchí-Navarro, S.; Martínez-Esteso, M.J.; Youssef, S.M.; Casado-Vela, J.; Vera-Urbina, J.C.; Sellés-Marchart, S.; Bru-Martínez, R.; Pedreño, M.A. Suspension-Cultured Plant Cells as a Tool to Analyze the Extracellular Proteome. *Methods Mol. Biol.* **2014**, *1072*, 407–433. [CrossRef] [PubMed]
9. Michalak, M. Plant Extracts as Skin Care and Therapeutic Agents. *Int. J. Mol. Sci.* **2023**, *24*, 15444. [CrossRef] [PubMed]
10. Pérez-Rivero, C.; López-Gómez, J.P. Unlocking the Potential of Fermentation in Cosmetics: A Review. *Fermentation* **2023**, *9*, 463. [CrossRef]
11. Herman, A.; Herman, A.P. Biological Activity of Fermented Plant Extracts for Potential Dermal Applications. *Pharmaceutics* **2023**, *15*, 2775. [CrossRef] [PubMed]
12. Wijesekara, T.; Xu, B. Health-Promoting Effects of Bioactive Compounds from Plant Endophytic Fungi. *J. Fungi* **2023**, *9*, 997. [CrossRef] [PubMed]
13. Arora, N.; Patel, A.; Mehtani, J.; Pruthi, P.A.; Pruthi, V.; Poluri, K.M. Co-Culturing of Oleaginous Microalgae and Yeast: Paradigm Shift towards Enhanced Lipid Productivity. *Environ. Sci. Pollut. Res.* **2019**, *26*, 16952–16973. [CrossRef] [PubMed]
14. Bokelmann, J.M. Holy Basil/Tulsi (Ocimum Tenuiflorum/Sanctum). In *Medicinal Herbs in Primary Care*; Elsevier Science: Amsterdam, The Netherlands, 2022; pp. 437–440.
15. Sen, K.; Goyal, M.; Mukopadayay, S. Review on Phytochemical and Pharmacological, Medicinal Properties of Holy Basil (*Ocimum sanctum* L.). *Int. J. Health Sci.* **2022**, *6*, 7276–7286. [CrossRef]
16. Halisky, P.M.; Webster, R.K. Heterothallism in *Ustilago cynodontis* (Pass.) Henn. *Nature* **1963**, *197*, 919–920. [CrossRef]
17. Ernst, P.; Saur, K.M.; Kiefel, R.; Niehoff, P.J.; Weskott, R.; Büchs, J.; Jupke, A.; Wierckx, N. Balancing PH and Yield: Exploring Itaconic Acid Production in *Ustilago cynodontis* from an Economic Perspective. *Biotechnol. Biofuels Bioprod.* **2024**, *17*, 103. [CrossRef] [PubMed]
18. Morita, T.; Konishi, M.; Fukuoka, T.; Imura, T.; Kitamoto, D. Identification of *Ustilago cynodontis* as a New Producer of Glycolipid Biosurfactants, Mannosylerythritol Lipids, Based on Ribosomal DNA Sequences. *J. Oleo Sci.* **2008**, *57*, 549–556. [CrossRef] [PubMed]
19. Hosseinpour Tehrani, H.; Tharmasothirajan, A.; Track, E.; Blank, L.M.; Wierckx, N. Engineering the Morphology and Metabolism of PH Tolerant *Ustilago cynodontis* for Efficient Itaconic Acid Production. *Metab. Eng.* **2019**, *54*, 293–300. [CrossRef] [PubMed]
20. Geiser, E.; Wiebach, V.; Wierckx, N.; Blank, L.M. Prospecting the Biodiversity of the Fungal Family Ustilaginaceae for the Production of Value-Added Chemicals. *Fungal Biol. Biotechnol.* **2014**, *1*, 2. [CrossRef] [PubMed]
21. Newman, N.; Rajangam, A.; Talavera-Adame, D.; Sidhu, H. System and Method for the Production, Formulation and Use of Conditioned Media, Cultured Cells and the Factors Included Therein. U.S. Patent 11,473,117 B2, 18 October 2022.
22. Ullmann, L.; Wibberg, D.; Busche, T.; Rückert, C.; Müsgens, A.; Kalinowski, J.; Blank, L.M. Seventeen Ustilaginaceae High-Quality Genome Sequences Allow Phylogenomic Analysis and Provide Insights into Secondary Metabolite Synthesis. *J. Fungi* **2022**, *8*, 269. [CrossRef] [PubMed]
23. Li, H.; Durbin, R. Fast and Accurate Short Read Alignment with Burrows–Wheeler Transform. *Bioinformatics* **2009**, *25*, 1754–1760. [CrossRef] [PubMed]

24. Danecek, P.; Bonfield, J.K.; Liddle, J.; Marshall, J.; Ohan, V.; Pollard, M.O.; Whitwham, A.; Keane, T.; McCarthy, S.A.; Davies, R.M.; et al. Twelve Years of SAMtools and BCFtools. *Gigascience* **2021**, *10*, giab008. [CrossRef] [PubMed]
25. Talevich, E.; Shain, A.H.; Botton, T.; Bastian, B.C. CNVkit: Genome-Wide Copy Number Detection and Visualization from Targeted DNA Sequencing. *PLoS Comput. Biol.* **2016**, *12*, e1004873. [CrossRef] [PubMed]
26. Stanke, M.; Diekhans, M.; Baertsch, R.; Haussler, D. Using Native and Syntenically Mapped CDNA Alignments to Improve de Novo Gene Finding. *Bioinformatics* **2008**, *24*, 637–644. [CrossRef] [PubMed]
27. Stanke, M.; Schöffmann, O.; Morgenstern, B.; Waack, S. Gene Prediction in Eukaryotes with a Generalized Hidden Markov Model That Uses Hints from External Sources. *BMC Bioinform.* **2006**, *7*, 62. [CrossRef] [PubMed]
28. Cingolani, P.; Platts, A.; Wang, L.L.; Coon, M.; Nguyen, T.; Wang, L.; Land, S.J.; Lu, X.; Ruden, D.M. A Program for Annotating and Predicting the Effects of Single Nucleotide Polymorphisms, SnpEff. *Fly* **2012**, *6*, 80–92. [CrossRef] [PubMed]
29. Rempel, A.; Wittler, R. SANS Serif: Alignment-Free, Whole-Genome-Based Phylogenetic Reconstruction. *Bioinformatics* **2021**, *37*, 4868–4870. [CrossRef] [PubMed]
30. Zemach, A.; Plaza, M.R.; Lee, B.S.; Little Dog, L.; Santiago-Rodriguez, E.; Simmons, D.; Palomares, M.; Talavera-Adame, D.; Newman, N. From Metabolomics to Function: Ranking Plant Stem Cell Metabolomes for Use in Health and Cosmetics. *Biomolecules* **2026**, *16*, 695. [CrossRef] [PubMed]
31. Bonini, P.; Kind, T.; Tsugawa, H.; Barupal, D.K.; Fiehn, O. Retip: Retention Time Prediction for Compound Annotation in Untargeted Metabolomics. *Anal. Chem.* **2020**, *92*, 7515–7522. [CrossRef] [PubMed]
32. Tsugawa, H.; Cajka, T.; Kind, T.; Ma, Y.; Higgins, B.; Ikeda, K.; Kanazawa, M.; VanderGheynst, J.; Fiehn, O.; Arita, M. MS-DIAL: Data-Independent MS/MS Deconvolution for Comprehensive Metabolome Analysis. *Nat. Methods* **2015**, *12*, 523–526. [CrossRef] [PubMed]
33. Sumner, L.W.; Amberg, A.; Barrett, D.; Beale, M.H.; Beger, R.; Daykin, C.A.; Fan, T.W.-M.; Fiehn, O.; Goodacre, R.; Griffin, J.L.; et al. Proposed Minimum Reporting Standards for Chemical Analysis. *Metabolomics* **2007**, *3*, 211–221. [CrossRef] [PubMed]
34. Xia, J.; Psychogios, N.; Young, N.; Wishart, D.S. MetaboAnalyst: A Web Server for Metabolomic Data Analysis and Interpretation. *Nucleic Acids Res.* **2009**, *37*, W652–W660. [CrossRef] [PubMed]
35. Blois, M.S. Antioxidant Determinations by the Use of a Stable Free Radical. *Nature* **1958**, *181*, 1199–1200. [CrossRef]
36. Talavera-Adame, D.; Palomares, M.; Plaza, M.; Rogowski, N.; Lee, B.S.; Zemach, A.; Newman, N. Novel, Reproducible, Consortia Factors Derived from Adipose Stem Cells for Burn Wound Treatment. *Stem Cells Cloning* **2025**, *18*, 63–72. [CrossRef] [PubMed]
37. Feng, L.-L.; Xin, W.-N.; Tian, X.-L. MALAT1 Modulates MiR-146's Protection of Microvascular Endothelial Cells against LPS-Induced NF-KB Activation and Inflammatory Injury. *Innate Immun.* **2019**, *25*, 433–443. [CrossRef] [PubMed]
38. Sanchez, B.; Li, L.; Dulong, J.; Aimond, G.; Lamartine, J.; Liu, G.; Sigaudo-Roussel, D. Impact of Human Dermal Microvascular Endothelial Cells on Primary Dermal Fibroblasts in Response to Inflammatory Stress. *Front. Cell Dev. Biol.* **2019**, *7*, 44. [CrossRef] [PubMed]
39. Hou, H.; Li, J.; Wang, J.; Hou, R.; Li, J.; Zhang, K. Abnormal Dermal Microvascular Endothelial Cells in Psoriatic Excessive Angiogenesis. *Microvasc. Res.* **2024**, *155*, 104718. [CrossRef] [PubMed]
40. Chan, E.L.; Murphy, J.T. Reactive Oxygen Species Mediate Endotoxin-Induced Human Dermal Endothelial NF-KB Activation. *J. Surg. Res.* **2003**, *111*, 120–126. [CrossRef] [PubMed]
41. Pullar, J.; Carr, A.; Vissers, M. The Roles of Vitamin C in Skin Health. *Nutrients* **2017**, *9*, 866. [CrossRef] [PubMed]
42. Kubo, I.; Fujita, K.; Lee, S.H. Antifungal Mechanism of Polygodial. *J. Agric. Food Chem.* **2001**, *49*, 1607–1611. [CrossRef] [PubMed]
43. Park, H.; Ko, R.; Seo, J.; Ahn, G.Y.; Choi, S.; Kwon, M.; Lee, S.Y. Octyl Gallate Has Potent Anti-inflammasome Activity by Directly Binding to NLRP3 LRR Domain. *J. Cell. Physiol.* **2024**, *239*, e31196. [CrossRef] [PubMed]
44. Michalak, K.P.; Michalak, A.Z. Understanding Chronic Inflammation: Couplings between Cytokines, ROS, NO, Ca_i^{2+}, HIF-1α, Nrf2 and Autophagy. *Front. Immunol.* **2025**, *16*, 1558263. [CrossRef] [PubMed]
45. Morgan, M.J.; Liu, Z. Crosstalk of Reactive Oxygen Species and NF-KB Signaling. *Cell Res.* **2011**, *21*, 103–115. [CrossRef] [PubMed]
46. Liu, S.; Liu, J.; Wang, Y.; Deng, F.; Deng, Z. Oxidative Stress: Signaling Pathways, Biological Functions, and Disease. *MedComm* **2025**, *6*, e70268. [CrossRef] [PubMed]
47. Liu, T.; Zhang, L.; Joo, D.; Sun, S.-C. NF-KB Signaling in Inflammation. *Signal Transduct. Target. Ther.* **2017**, *2*, 17023. [CrossRef] [PubMed]
48. Shalaby, S.; Horwitz, B.A. Plant Phenolic Compounds and Oxidative Stress: Integrated Signals in Fungal–Plant Interactions. *Curr. Genet.* **2015**, *61*, 347–357. [CrossRef] [PubMed]
49. Foyer, C.H.; Noctor, G. Redox Homeostasis and Antioxidant Signaling: A Metabolic Interface between Stress Perception and Physiological Responses. *Plant Cell* **2005**, *17*, 1866–1875. [CrossRef] [PubMed]
50. López-Martínez, L.X.; Aguirre-Delgado, A.; Saenz-Hidalgo, H.K.; Buenrostro-Figueroa, J.J.; García, H.S.; Baeza-Jiménez, R. Bioactive Ingredients of Huitlacoche (Ustilago Maydis), a Potential Food Raw Material. *Food Chem. Mol. Sci.* **2022**, *4*, 100076. [CrossRef] [PubMed]

51. Shim, K.S.; Kim, H.J.; Ji, K.Y.; Jung, D.H.; Park, S.H.; Song, H.K.; Kim, T.; Kim, K.M. Rosmarinic Acid Ameliorates Dermatophagoides Farinae Extract-Induced Atopic Dermatitis-like Skin Inflammation by Activating the Nrf2/HO-1 Signaling Pathway. *Int. J. Mol. Sci.* **2024**, *25*, 12737. [CrossRef] [PubMed]
52. Picerno, P.; Autore, G.; Marzocco, S.; Meloni, M.; Sanogo, R.; Aquino, R.P. Anti-Inflammatory Activity of Verminoside from Kigelia Africana and Evaluation of Cutaneous Irritation in Cell Cultures and Reconstituted Human Epidermis. *J. Nat. Prod.* **2005**, *68*, 1610–1614. [CrossRef] [PubMed]
53. Ju, S.; Tan, Y.; Wang, Q.; Zhou, L.; Wang, K.; Wen, C.; Wang, M. Antioxidant and Anti-inflammatory Effects of Esculin and Esculetin (Review). *Exp. Ther. Med.* **2024**, *27*, 248. [CrossRef] [PubMed]
54. Yi, G.; Zhang, R.; Li, M.; Song, X.; Li, S. Atractylenolide-III Attenuates Osteoarthritis by Repolarizing Macrophages through Inactivating TLR4/NF-KB Signaling. *Int. Immunopharmacol.* **2024**, *129*, 111629. [CrossRef] [PubMed]
55. Jin, B.; Chen, Y.; Wang, J.; Chen, Y.; Zhang, M.; Huang, J.; Wang, Y. Costunolide Alleviates Hyperglycaemia-Induced Diabetic Cardiomyopathy via Inhibiting Inflammatory Responses and Oxidative Stress. *J. Cell. Mol. Med.* **2023**, *27*, 831–845. [CrossRef] [PubMed]
56. Potgieter, L.; Feurtey, A.; Dutheil, J.Y.; Stukenbrock, E.H. On Variant Discovery in Genomes of Fungal Plant Pathogens. *Front. Microbiol.* **2020**, *11*, 626. [CrossRef] [PubMed]
57. Agrawal, R.; Hu, A.; Bollag, W.B. The Skin and Inflamm-Aging. *Biology* **2023**, *12*, 1396. [CrossRef] [PubMed]
58. Papaccio, F.; D'Arino, A.; Caputo, S.; Bellei, B. Focus on the Contribution of Oxidative Stress in Skin Aging. *Antioxidants* **2022**, *11*, 1121. [CrossRef] [PubMed]

Disclaimer/Publisher's Note: The statements, opinions and data contained in all publications are solely those of the individual author(s) and contributor(s) and not of MDPI and/or the editor(s). MDPI and/or the editor(s) disclaim responsibility for any injury to people or property resulting from any ideas, methods, instructions or products referred to in the content.